IEEE Access
Multidisciplinary | Rapid Review | Open Access Journal

Received December 5, 2019, accepted March 4, 2020, date of publication March 16, 2020, date of current version March 25, 2020.

Digital Object Identifier 10.1109/ACCESS.2020.2980900

Microscale Flow Field Analysis and Flow Prediction Model Exploration of Dry Gas Seal

YAN WANG, YUNLU GE, GUOQING HUANG, QIONG HU, AND PENG HU
School of Mechanical and Ocean Engineering, Jiangsu Ocean University, Lianyungang 222005, China

Corresponding author: Yan Wang (qqwangyan2006@163.com)

This work was supported in part by the National Natural Science Foundation of China under Grant 51741504 and Grant 51805199, in part by the Natural Science Foundation of Jiangsu Province under Grant BK20191471, in part by the Qinglan Project in Jiangsu Province, and in part by the Six Talent Peaks in Jiangsu Province of Lianyungang City (521 Project) under Grant GDZB-076.

ABSTRACT The characteristics of high speed, high pressure, microscale, and rotating flow fields result in very complicated flow between the dynamic and static rings of a dry gas seal. In particular, the existence of a groove, dam, and weir further contribute to the uncertainty of a microscale flow field. Classically, the flow regime of pipe flow is determined based on the critical Reynolds number (Pipe model) while the rotating flow field is sometimes determined by the flow factor (Oval model). In this study, a new method was developed that can be used for prediction of flow regime of a dry gas seal rotating flow field based on a three-dimensional velocity component (Ellipsoid model). The aim was to make the given model reflect the flow regime more realistically based on the consideration of the axial velocity component. When modeling dry gas seal rotating flow fields, we showed that compared to the one-dimensional Pipe model and the two-dimensional Oval model, the three-dimensional Ellipsoid model proposed in this paper can produce more accurate results.

INDEX TERMS Ellipsoid model, flow regime, microscale, dry gas seal, rotating flow field.

NOMENCLATURE

h	Film thickness [mm]
h_g	Groove depth [μm]
N_g	Spiral groove number
N	Rotation speed [rpm]
P_{out}	Outlet pressure [MPa]
P_{in}	Inlet pressure [MPa]
r_i	Inner radius of the seal ring [mm]
r_o	Outer radius of the seal ring [mm]
r_g	Root radius of the seal ring [mm]
κ	Width ratio of the groove to the ridge
α	Helix angle [°]
Q	Leakage rate [m^3/h]
F	Opening force [kN]
ρ	Medium density [kg/m^3]
μ	Viscosity [Pa·s]
L	Characteristic length [m]
Re	Reynolds number
Re_c	Couette Reynolds number
Re_p	Poiseuille Reynolds number
Re_a	Perturbation Reynolds number
ω	Angular velocity [rad/s]
v	Average rotational linear velocity [m/s]
v_c	Circumferential linear velocity [m/s]
v_r	Mean radial velocity [m/s]
v_a	Axial velocity [m/s]
ξ	Flow factor
A	Flow area [m^2]
S	Contact circumference [m]
X	The critical Reynolds number corresponding to the Re_a
Γ_1, Γ_2	Periodic boundary condition

The associate editor coordinating the review of this manuscript and approving it for publication was Yunjie Yang.

I. INTRODUCTION

In 1979, Gabriel first proposed the spiral groove dry gas seal (S-DGS) based on the hydrostatic and hydrodynamic principle in [1]. Since then, many scholars in [2]–[5] have analyzed the performance of this structure using numerical and computational fluid dynamics methods. The quality of dry gas seal (DGS) performance analysis largely depends on the scientific definition of the flow regime of the microscale rotating flow field between the seal pairs. Typically, according to [6], [7], such a flow regime is mainly divided into

laminar and turbulent flow and determined as a function of the medium density, viscosity, hydraulic diameter, and flow velocity. The decision method based on the critical Reynolds number (Pipe model) for the pipe flow has been widely accepted, though the dry gas seal is a rotating flow field. The reasonable decision method of a microscale rotary flow field of DGS plays an important role in scientifically determining the hydrodynamic behavior.

In the calculation of a rotating flow field, many studies such as [8], [9] have been limited because of the lack of theoretical models or methods to accurately determine the flow regime. However, authors in [10], [11] have studied the characteristics of the DGS rotating flow field under different flow regimes. The results highlight significant variations in sealing characteristic parameters in the flow regime transition. The results tend to agree that the calculation of a turbulent regime will overestimate the peak value of the gas film pressure.

At present, it is still controversial whether the flow regime of a DGS rotating flow field is laminar or turbulent flow. When the inlet pressure is approximately 0.5 MPa and the maximum rotation speed is approximately 10000 rpm, scholars in [12], [13] tend to believe that the laminar regime is more consistent with the actual flow field. However, when the pressure is approximately 4.5 MPa, some scholars in [14], [15] suggest that the actual flow field is near the turbulent regime. Generally speaking, according to [16], [17], most studies have been conducted for a laminar flow in the film. Very few workers have been concerned with seals operating in the turbulent flow regime.

In [18], Brunetiere presented a flow factor method (Oval model) to determine pressure and velocities for laminar to turbulent isothermal flow in the mechanical seal interface. An original technique was proposed to characterize the fluid flow regime in the film while simultaneously considering the Couette and Poiseuille flows. Subsequently, scholars in [19], [20] have used this model to determine the flow regime between DGS pairs. However, although this model is more accurate than the Pipe model, the results are still inclined to support the conclusion of a laminar regime, even when conditions reach ultra-high speed.

In view of this, the Ellipsoid model was established based on a three-dimensional velocity component in this study. The circumferential, radial, and axial velocity components on DGS macro performance were investigated and the model was verified by analyzing the rotating flow field of the DGS under different geometric and operational parameters. The model is of benefit to further scientific research regarding DGSs and similar high-speed impeller equipment.

It is challenging to develop a comprehensive model that accurately reflects flow regime such that scientific theoretical calculations can be conducted. Addressing this challenge is the primary concern of this work presented. The objectives of this work can be summarized as follows:

- Characterization and modeling of flow regime and its transition in terms of macroscopic sealing performance, microscopic flow field characteristics, and three-dimensional velocity component;
- Development of an Ellipsoid model of space, based on the Brunetiere *et al.* model and the hydraulic diameter model defined in terms of the Reynolds number, and demonstration of its plausibility;
- Highlighting the importance of the axial velocity component in governing the flow regime of a DGS rotating flow field at high speed.

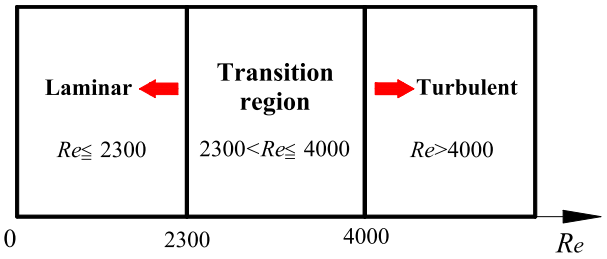

FIGURE 1. Pipe flow decision model (Pipe model).

II. EXISTING FLOW REGIME DECISION MODEL

A. PIPE FLOW DECISION MODEL

The Reynolds number (Re) represents the ratio of inertial force and viscous force in a flow field and is a dimensionless number used to determine the flow state of a viscous fluid. Formulated by O. Reynolds in 1883, it was expressed in the following manner:

$$Re = \frac{\rho UL}{\mu} \tag{1}$$

where ρ, U, and μ represent the medium density, pipe flow velocity, and viscosity, respectively, and L is the characteristic length. For example, if fluid flows through a circular pipe, L is the equivalent pipe diameter. Re can be used to distinguish laminar from turbulent flow: A small Re value means that the viscous force affects the flow field more than the inertial force. In this case, the disturbance of velocity in the flow field will be attenuated by the viscous force and the flow regime is considered laminar flow. In contrast, when Re is large, thus indicates that the flow is unstable. At this point, increasing velocity tends to develop, enhance, and eventually form a turbulent, irregular flow field. When studying the flow field parameters of a DGS, scholars in [21], [22] have directly chosen (1) for the flow regime analogy analysis: U is analogous to the average rotation linear velocity v (as shown in (2)) and L to the gas film thickness h.

$$v = \frac{N \times \pi \times 2\left(\frac{r_o + r_i}{2}\right) \times 10^{-3}}{60} \tag{2}$$

where N, r_o, and r_i represent the rotation speed, outer and inner radius of the seal ring, respectively. The calculation parameters were selected from Gabriel's classic in [1]: $\rho = 1.29$ kg/m^3, $\mu = 1.86 \times 10^{-5}$ Pa·s, $h = 3.05$ μm, and $N = 10380.8$ rpm. Using (1) results in a $Re = 15.65$.

Fig. 1 shows the flow regime decision model (Pipe model) in pipe flow. When $Re \leqq 2300$, it is a laminar regime; when

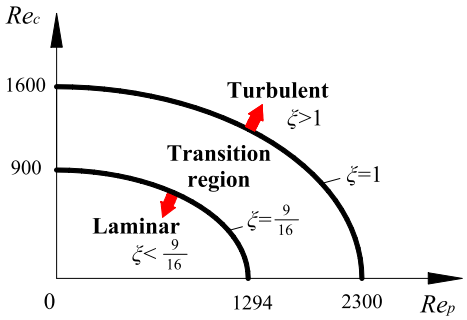

FIGURE 2. Flow factor decision model (Oval model).

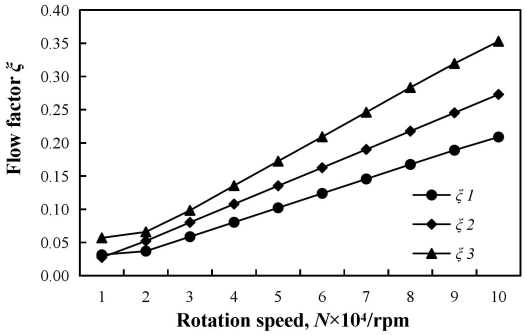

FIGURE 3. Relation between rotation speed and flow constant (ξ_1: $h = 5\mu$m, $h_g = 5\mu$m, $P_{in} = 2$MPa; ξ_2: $h = 4\mu$m, $h_g = 2\mu$m, $P_{in} = 2$MPa; ξ_3: $h = 4\mu$m, $h_g = 5\mu$m, $P_{in} = 3$MPa).

Re is between 2300 and 4000, it is a transitional regime, and when $Re > 4000$; it is a turbulent regime. According to the Pipe model, the aforementioned result ($Re = 15.65$) is still far less than 2300 even if the rotation speed reaches 1×10^6 rpm ($Re = 1565$). At such a ultra-high speed, the decision result of the model is still laminar flow, so the the accuracy of the method to directly determine the flow regime of the rotating flow field based on the Pipe model is debatable.

B. FLOW FACTOR MODEL

Referring to Brunetiere's decision method of a rotating flow field of a mechanical seal in [18], this method is based on the flow factor ξ, which is defined as follows:

$$\begin{cases} \xi = \sqrt{\left(\dfrac{Re_c}{1600}\right)^2 + \left(\dfrac{Re_p}{2300}\right)^2} \\ Re_c = \dfrac{\rho v_c L}{\mu} \\ Re_p = \dfrac{\rho v_r L}{\mu} \end{cases} \tag{3}$$

where Re_c and Re_p are Reynolds numbers for the circumferential flow of Couette and the radial Poiseuille flow, respectively. v_c is the circumferential linear velocity of the end face and v_r is the mean radial velocity across the film. The geometric model corresponding to (3) can be represented by the Oval model with two equal-eccentricity ellipses, as shown in Fig. 2. It is stipulated that when $\xi < 9/16$, the fluid is in a laminar regime; when $9/16 \leqq \xi \leqq 1$, it is in a transitional regime; and when $\xi > 1$, it is in a turbulent regime. According to the results in [23], the maximum velocity v_{max} and radial velocity components v_r in the flow field can be directly obtained by Fluent software, and then the circumferential velocity components v_c can be obtained by formula $v_{\max}^2 = v_r^2 + v_c^2$. Under the calculation parameters in this paper, when $N = 10{,}380.8$ rpm, the calculated v_{max} and v_r are about 148.17 m/s and 98.05 m/s, respectively. So the corresponding $v_c = 111.09$ m/s can be obtained. By substituting this into (3), it can be obtained that $Re_c = 23.5$, $Re_p = 20.74$, and $\xi = 0.017 \ll 1$, which can be determined as laminar regime. It can be seen that the Oval model considering both the circumferential Couette flow and radial Poiseuille flow is more accurate than the Pipe model and can actually reflect the influence of pressure gradient and rotation factors in the rotating flow field.

TABLE 1. The critical speed corresponding to the two models.

	Decision parameter	Complete turbulence decision value	Critical speed
Pipe model	*Re*	4000	2.7×10^6
Oval model	ξ	1	6.0×10^5

Further research showed that, even at different film thicknesses, groove depths, and pressures, the increase in rotation speed has a basically linear relationship with flow factors as shown in Fig. 3. Through the fitting calculation of the aforementioned parameters, it can be known that the turbulence condition ($\xi \approx 1$) can only be reached theoretically when the rotation speed N reaches 6×10^5 rpm(critical speed), and the critical speed corresponding to the Pipe model can be obtained by the same method, as shown in Table 1. Although the critical speed of the Oval model is much lower than that of the Pipe model, it is still at a high speed.

III. PROBLEM BACKGROUND

A. DISCOVERY OF MACROSCOPIC DISTURBANCE PHENOMENON AT HIGH SPEEDS

Through a systematic study of DGS performance parameters, Wang *et al.* [24] found that, similar to the micro-vibration phenomenon of gas bearing, the opening force and leakage rate of DGS are not positively correlated to rotation speed; the representative trend is shown in Fig. 4 (The numerical model, geometric parameters and boundary conditions are consistent with this paper).

As can be seen, both the opening force and leakage rate have two inflection points with the continuous increase in rotation speed. Further research also found that, particularly at a high pressure and with a large film thickness and small groove depth, the disturbance phenomenon (non-positive correlation between performance parameters and rotation speed) is more significant. The reason for this may be that with

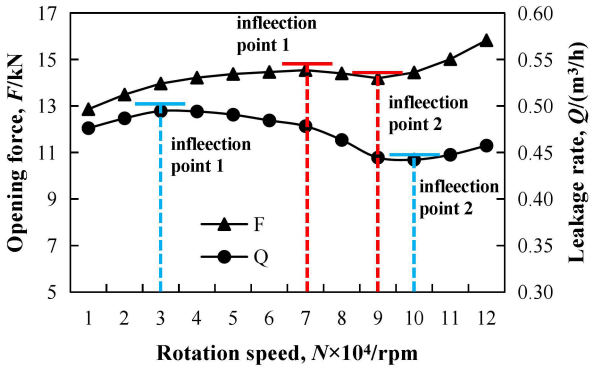

FIGURE 4. Macroscopic parameter variation rule of a DGS at different rotation speeds ($h = 5\mu$m, $h_g = 5\mu$m, $P_{in} = 2$MPa).

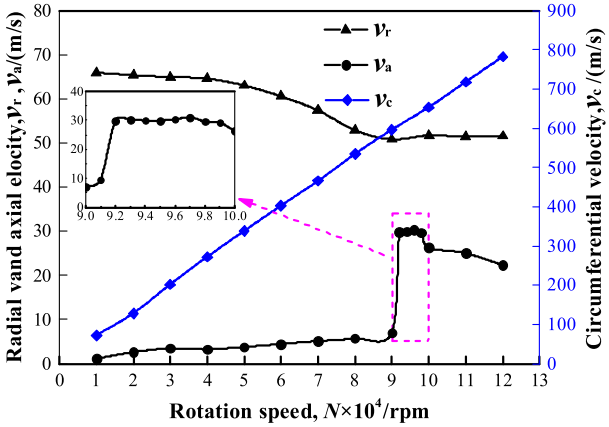

FIGURE 5. Evolution of a microscale three-dimensional velocity field ($h = 5\mu$m, $h_g = 4\mu$m, $P_{in} = 2$MPa).

the change in specific operational and geometric parameters, some uncertain fluctuation factors appear in fluid flow at a microscale. Furthermore, with the continuous increase in the rotation speed, the relationship between the macrosealing performance parameters and the rotation speed returns to a positive correlation. This indicates that there must be some favorable factors in the microcosmic flow field to promote the dynamic pressure effect at this time, and then the macroscopic phenomenon of increasing opening force and increasing leakage rate appears.

B. DISCOVERY OF AN AXIAL VELOCITY COMPONENT AT HIGH SPEEDS

In view of the fluctuation of macroscopic performance parameters at high speeds, our research group further analyzed the evolutionary mechanism of the microscopic velocity field with the increase in rotation speed. As shown in Fig. 5, the variation trend of the three-dimensional velocity flow field composed of circumferential, radial, and axial component directions with the rotation speed was analyzed. In the rotating flow field, the circumferential velocity component has the largest magnitude and basically a linear relationship with the increase in rotation speed, followed by the radial velocity component. The difference is that, with the increase in rotation speed, the radial velocity component

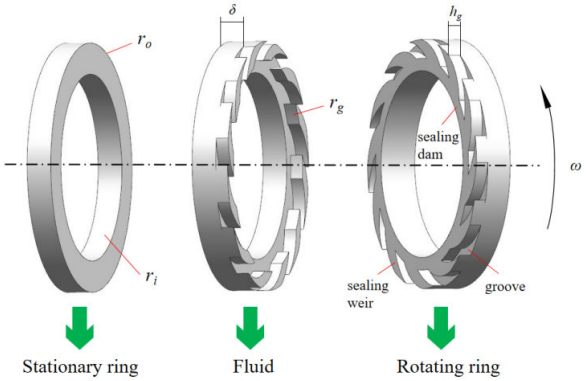

FIGURE 6. Diagram of S-DGS.

shows an obvious fluctuation phenomenon. This indicates that there is a critical point for the effect of rotation speed on the radial velocity component. Before and after the critical point, the increase in rotation speed has the opposite effect on the radial velocity component. The most important feature is the change mechanism of the axial velocity component: the magnitude of the axial velocity component is the smallest and can be basically ignored. It increases slowly with the increase in rotation speed, but when the rotation speed continues to increase and reaches the macroscopic critical value (that is, when the performance parameters and the speed of the inverse proportional relationship, as shown in Fig. 5, about 9.2×10^4 rpm), the axial velocity component will rapidly increase to an order of magnitude that can no longer be ignored.

Therefore, by referring to the Oval model, it can be inferred that the role of the axial velocity component should also be considered at a high rotation speed as the axial velocity component may be caused by the unsteady flow of fluid at this speed. The specific mechanism is elaborated in detail in the following.

IV. BASIC ASSUMPTIONS AND CALCULATION MODEL

To systematically explain the condition of the macroscopic disturbance phenomenon and its internal relation with the mesoscopic flow field, the geometric parameters of S-DGS in [1] were selected as the modeling basis and systematically studied, as shown in Table 2 and Fig. 6.

A. BASIC ASSUMPTIONS

For the numerical analysis, several assumptions in [25], [26] were employed as follow

- The medium between the sealing pairs is in a fluid friction state and can form a stable gas film.
- There is no relative slip condition at the interface.
- The effect of sealing end surface roughness is not considered.
- The influence of temperature and pressure on viscosity is ignored.
- The gas between the sealing pairs has the characteristics of a continuous medium and can be regarded as such.

TABLE 2. Parameters used during the systematically is.

Geometric parameters and operating parameters	
Outer radius of the seal ring r_o [mm]	77.78
Root radius of the seal ring r_g [mm]	69
Inner radius of the seal ring r_i [mm]	58.42
Width ratio of the groove to the ridge κ	1
Groove depth h_g [μm]	2, 3, 4, 5
Film thickness h [μm]	3, 4, 5, 6
Medium	Ideal gas
Inlet pressure p_i [MPa]	0.5, 1, 2, 3, 4
Outlet pressure p_o [MPa]	0.1013
Rotation speed $N \times 10^{-4}$[rpm]	1-12(integers)
Spiral groove number N_g	12
Helix angle α [°]	15

- The fluid in the gas film obeys the isothermal and ideal gas model.
- Both the rotating and stationary rings are rigid bodies.
- The inertial force and blocking effect are not considered.

Study in [2] shows that the performance parameters of dry gas seal are easily affected by the slip flow effect at low speed (≦500 rpm) and low pressure (≦0.303 MPa). The slip flow effect results in the decrease of opening performance and the increase of leakage. In view of the high speed and high pressure conditions in this paper, the influence of slip flow can be ignored. Furthermore, the fluid-solid coupling effect is mainly based on the consideration of the thermal deformation of the sealing ring. In order to simplify the flow field calculation, the influence of this factor is not considered temporarily.

The results in [18] on fluid film of mechanical seals show that inertial terms remain insignificant in the majority of the cases studied. Moreover, the density of gases is much lower than that of fluids. Hence, it seems reasonable to neglect inertial forces even at high speeds.

The blocking effect occurs when the gas velocity reaches supersonic, which causes the outlet pressure of the sealed gas to rise, thereby affecting the opening force. Study in [27] shows that when the pressure is 10 MPa and the rotation speed is 5×10^4 rpm, the blocking effect reduces the opening force by 6% and leakage by 70.7%. However, when the pressure is 5 MPa and the rotation speed reaches 2×10^5 rpm, the opening force increases by only 4% and the leakage increases by only 8%. It can be seen that, compared to the operational conditions in this study (the highest speed was 1.2×10^5 rpm and the maximum pressure was 4 MPa), the blocking effect can be ignored.

B. NUMERICAL MODEL

To further study the internal evolution law of a microscale flow field, when the specific flow regime of the DGS rotating flow field is uncertain, laminar and turbulent regimes are, respectively, selected for analysis.

The continuity equation under the steady state flow of axisymmetric condition is stated by (4)

$$\frac{\partial}{\partial r}(\rho r V_r) + \frac{\partial}{\partial z}(\rho r V_z) = 0 \tag{4}$$

The Navier-Stokes equation applicable to a thin fluid film, including circumferential, radial and axial directions, is shown as (5).

$$\begin{cases} V_r \dfrac{\partial V_r}{\partial r} + V_z \dfrac{\partial V_z}{\partial z} - \dfrac{V_\theta^2}{r} = -\dfrac{1}{\rho}\dfrac{\partial P}{\partial r} + \dfrac{1}{\rho}\dfrac{\partial}{\partial z}\left(\mu \dfrac{\partial V_r}{\partial z}\right) \\ V_r \dfrac{\partial V_\theta}{\partial r} + V_z \dfrac{\partial V_\theta}{\partial z} - \dfrac{V_\theta V_r}{r} = \dfrac{1}{\rho}\dfrac{\partial}{\partial z}\left(\mu \dfrac{\partial V_\theta}{\partial z}\right) \\ \dfrac{1}{\rho}\dfrac{\partial P}{\partial z} = 0 \end{cases} \tag{5}$$

Reynolds average method is a common method to study turbulence. This paper uses Reynolds average method to solve Navier-Stokes equation and describe turbulence regime. In view of the high computational accuracy of RNG (renormalization group) method and the better simulation effect of strong curl flow field than other methods, the RNG k-ε turbulent model was adopted. This model was established in [28] by Yakhot and Orzag and is applicable to a low Reynolds number as shown in (6) and (7).

$$\frac{\partial(\rho k)}{\partial t} + \frac{\partial(\rho k u_i)}{\partial x_i} = \frac{\partial}{\partial x_j}\left[\alpha_k u_{eff} \frac{\partial k}{\partial x_j}\right] + G_k + \rho\varepsilon \tag{6}$$

$$\frac{\partial(\rho k)}{\partial t} + \frac{\partial(\rho \varepsilon u_i)}{\partial x_i} = \frac{\partial}{\partial x_j}\left[\alpha_k u_{eff} \frac{\partial k}{\partial x_j}\right] + \frac{C_{1\varepsilon}^*}{k} G_k + C_{2\varepsilon}\rho\frac{\varepsilon^2}{k} \tag{7}$$

where, the relevant parameters and specific values are as follows:

$$\begin{aligned} \mu_{eff} &= \mu + \mu_i, \\ \mu_i &= \rho C_\mu k^2/\varepsilon, \\ C_\mu &= 0.0845, \quad \alpha_k = \alpha_\varepsilon = 1.39, \\ C_{1\varepsilon}^* &= C_{1\varepsilon} - \frac{\eta(1-\eta/\eta_o)}{1+\beta\eta^3} C_{1\varepsilon} = 1.42, \\ C_{2\varepsilon} &= 1.68, \quad \eta = \left(2E_{ij}\cdot E_{ij}\right)^{1/2} k/\varepsilon, \\ E_{ij} &= 0.5\left(\frac{\partial u_i}{\partial x_j} + \frac{\partial u_j}{\partial x_i}\right), \\ \eta_o &= 4.377, \quad \beta = 0.012 \end{aligned}$$

According to [10], the opening force can be calculated from expression as shown in (8).

$$F_o = \iint_A p dA = \int_{r_i}^{r_o} 2\pi p(r,\theta) r dr \tag{8}$$

Confirm the continuity hypothesis according to the previous part, the leakage rate of the DGS can be computed as

$$Q = \frac{h^3 r}{12\mu p_i} \int_0^{2\pi} \frac{\partial p}{\partial r} p d\theta \tag{9}$$

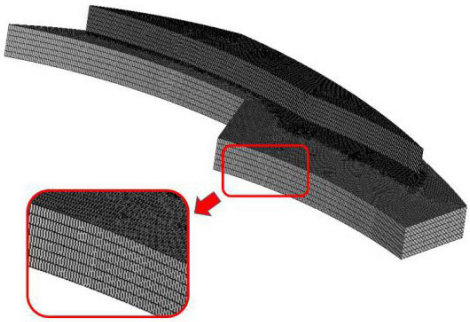

FIGURE 7. Mesh generation.

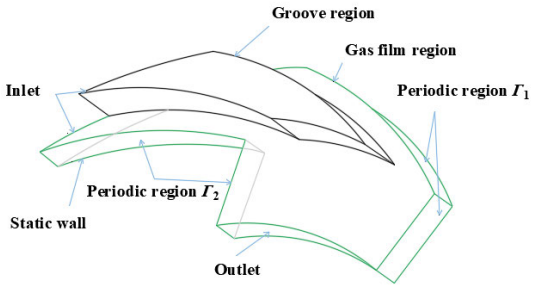

FIGURE 8. Geometric structure of spiral groove.

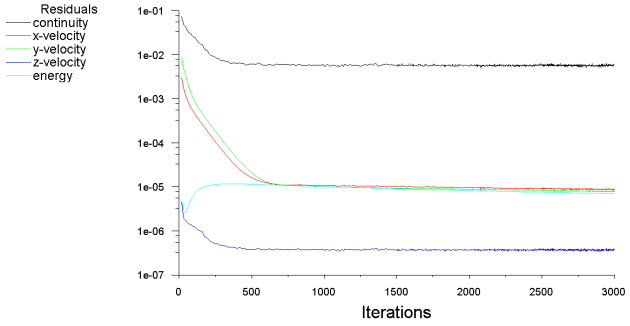

FIGURE 9. Convergence curve.

TABLE 3. Comparison of F under different film thickness.

h/μm	Opening force, F/N			Deviation	
	[30]	[14]	Calculated value	[30]	[14]
2.03	35.67	35.17	34.62	2.94%	1.56%
3.05	31.62	31.50	31.08	1.71%	1.33%
5.08	29.35	29.37	28.93	1.44%	1.50%

C. GRID AND BOUNDARY SETTINGS

The three-dimensional DGS model is characterized by a ratio of the sealing radial direction to the film thickness greater than 10,000 times, which is difficult in generating grids and can readily cause distortion in the calculation. In this study, the method of successive stretching of a grid was adopted to better address the problems of grid division and boundary condition setting. The groove and film regions were divided into six and ten layer meshes, respectively. The grid model (horizontal magnification of 10,000 times) is shown in Fig. 7.

In [2], [29], there are two kinds of boundary conditions, i.e. mandatory pressure boundary conditions and periodic boundary conditions. The outer diameter position of the groove inlet was the high-pressure side, represented by P_{out}, which was the external variable pressure. The inner diameter position of the groove outlet was the low-pressure side, represented by P_{in}, which was the constant atmospheric pressure.

Because the distribution of spiral grooves is periodic and symmetrical, the spiral groove area within a cycle was selected for the modeling and calculation, as shown in Fig. 8. The boundary conditions in the calculated region were considered as follows:

The pressure at the symmetric boundary Γ_1 and Γ_2 is equal:

$$\begin{cases} p\,|\Gamma_1 = p\,|\Gamma_2 \\ p\left(\theta + 2\pi/N_g\right) = p\left(\theta\right) \end{cases} \tag{10}$$

According to the mass flow conservation principle, by symmetrical boundary Γ_1 and Γ_2 mass flow should be equal:

$$\begin{cases} q\,|\Gamma_1 = q\,|\Gamma_2 \\ q\left(\theta + 2\pi/N_g\right) = q\left(\theta\right) \end{cases} \tag{11}$$

The solution method is as follows: Fluent 3D single-precision solver was selected as the solver, SIMPLEC algorithm (the cross-correction relationship between pressure and velocity is used to enforce the conservation of mass and obtain the pressure field) was used for pressure and velocity coupling, central difference scheme was used for dispersion term discrete format, and second-order upwind scheme was used for convection term discrete format to improve the accuracy of calculation results. The iterative accuracy of the model was set as 1×10^{-5}. The resulting convergence residual curve is shown in Fig. 9.

V. SIMULATION ANALYSIS

A. SIMULATION CALCULATION CLOUD MAP

Fig. 10 shows the pressure distribution and velocity distribution of the S-DGS with two flow regimes. It can be seen clearly from the cloud map, the pressure and velocity distributions have some deviation under different flow regimes. Under the parameters studied, the pressure in the turbulent regime is slightly higher than that in the laminar regime (2.583 MPa $>$ 2.341 MPa), and the velocity in a laminar regime is slightly higher than that in a turbulent regime (108.6 m/s $>$ 97.93 m/s). It is obvious that the specific pressure and velocity values of the two flow regimes are related to the selection of specific parameters. This is consistent with the following research and analysis conclusions.

B. VERIFICATION OF SIMULATION METHOD

In order to verify the numerical simulations, the parameters in [14], [30] were selected for calculation. The opening force F was taken as the target parameter and the compared values are shown in Table 3.

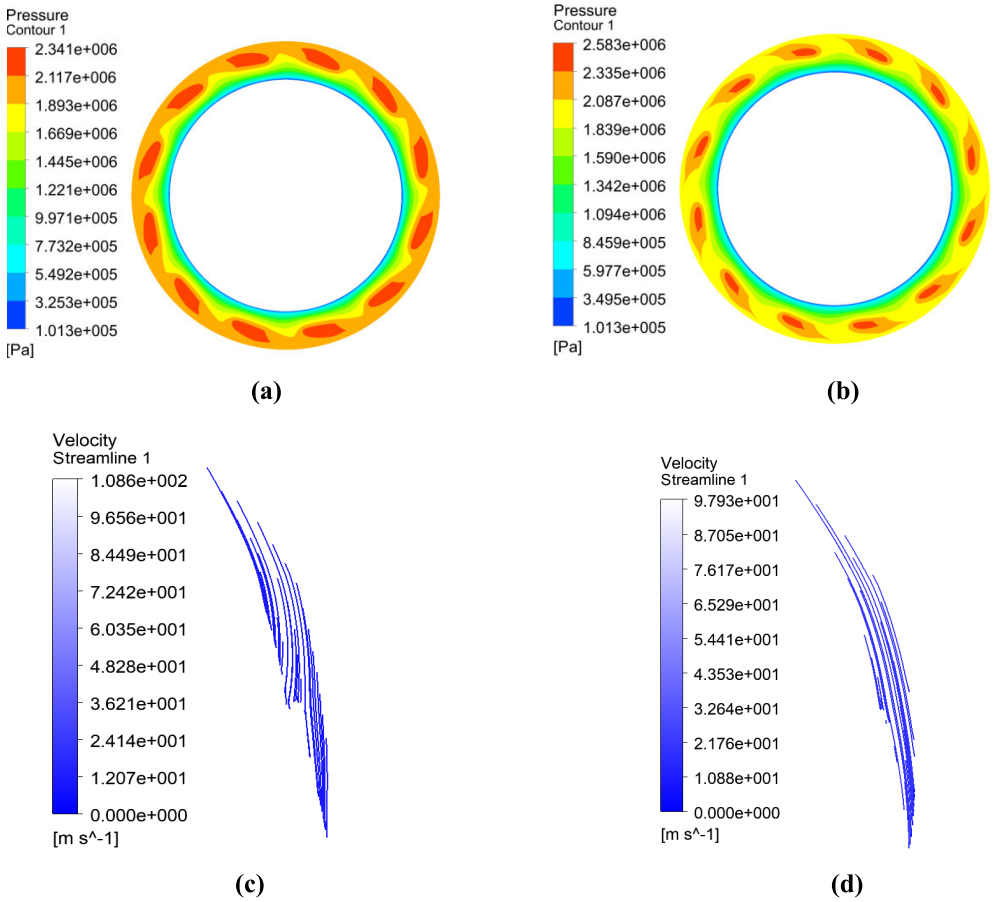

FIGURE 10. Pressure and velocity distribution with different flow regimes (P_{in} = 2 MPa, h = 3 μm, h_g = 4 μm, N = 1 × 10^4 rpm); (a) Pressure distribution in the laminar regime; (b) Pressure distribution in the turbulent regime; (c) Velocity distribution in the laminar regime; (d) Velocity distribution in the turbulent regime.

As presented in Table 3, the opening forces obtained from the numerical methods in this study are in good agreement with the values in the literature for different film thicknesses. The maximum deviation is within 3%, and the variation trend with film thickness is also found to match closely with the literature.

C. MACROSCOPIC DISTURBANCE PHENOMENON

1) UNDER DIFFERENT PRESSURES

Fig. 11(a) and (b) show the change trend of opening force and leakage rate of two flow regimes under different pressures, respectively. As can be seen, when the rotation speed is low, the opening forces of the two flow regimes under different pressures are basically the same and the leakage rate of the laminar regime is slightly higher than that of the turbulent regime. With an increase in pressure and rotation speed, the macroscopic performance difference between two flow regimes is increasingly obvious and gradually increases. In terms of macroscopic disturbance phenomenon, the decreasing trend of the opening force and leakage rate in the turbulent regime occurs earlier than that of the laminar regime. In other words, macroscopic performance parameters show a weak inflection point phenomenon in the turbulent regime.

It can be seen that the higher the pressure and rotation speed, the more obvious the influence of disturbance factors on the opening force and leakage rate.

2) AT DIFFERENT FILM THICKNESSES

Similar to the pressure, it can be seen from Fig. 12 that the change in film thickness has an obvious influence on the opening force and leakage rate and the law of action under the two flow regimes is basically the same. The leakage rate in the laminar regime is always greater than that in the turbulent regime; the difference with an increase in speed also increases. In the laminar regime, the opening force continues to increase with the increase in rotation speed and the smaller the film thickness, the larger the growth amplitude. In the case of the turbulent regime, the opening force shows the fluctuation trend of upward, downward, and upward. At this time, the inflection point is obvious, and the leakage rate also shows a corresponding fluctuation trend. However, in terms of the overall trend, the larger the film thickness, the more obvious the fluctuation range.

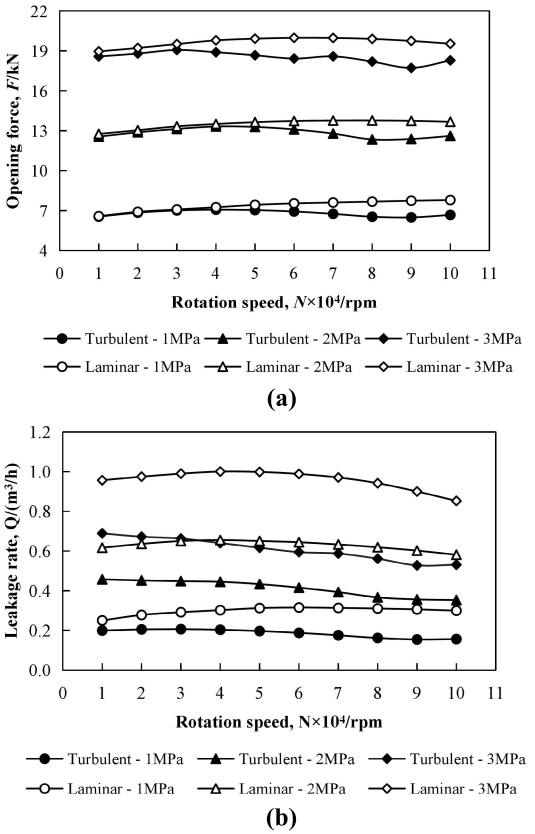

FIGURE 11. Performance comparison of two flow regimes under different pressures ($h = 5\mu$m, $h_g = 4\mu$m); (a) effect of pressure change on opening force; (b) effect of pressure change on leakage rate.

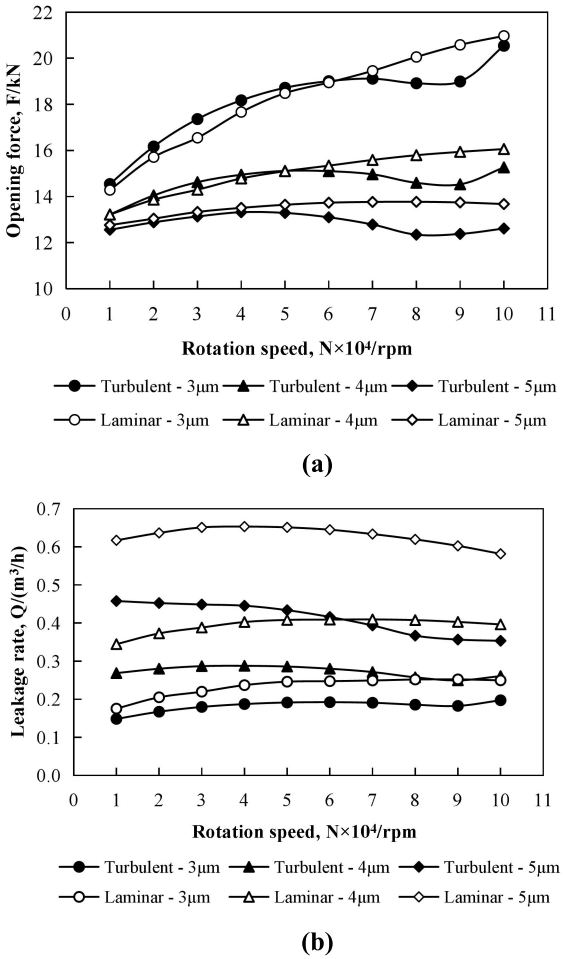

FIGURE 12. Performance comparison of two flow regimes at different film thicknesses ($P_{in} = 2$MPa, $h_g = 4\mu$m); (a) effect of the film thickness change on the opening force; (b) effect of the film thickness change on the leakage rate.

3) AT DIFFERENT GROOVE DEPTHS

As shown in Fig. 13, when the groove depth changes, the laminar regime is greater than the turbulent regime in terms of leakage rate. However, the opening force changes are slightly more complex and obviously affected by groove depth. The deeper the groove depth, the smaller the fluctuation of the opening force in the turbulent regime and the smaller the difference with the corresponding opening force in the laminar regime. Further analysis shows that when the groove depth is shallower and the rotation speed is higher, the fluctuation amplitude of the performance parameters in the turbulent regime is larger and the fluctuation trend is more obvious.

In summary, the fluid flow at a microscale of DGS is complex and the influence rule of the laminar and turbulent regimes on the sealing performance parameters is basically the same. The differences are mainly reflected in the slight differences in specific values and the phenomenon of multiple inflection points of performance parameters in the turbulent regime.

D. INHERENT RELATION BETWEEN THE MESOSCOPIC FLOW FIELD AND MACROSCOPIC DISTURBANCE PHENOMENON

To obtain the inherent relation and regularity between the macroscopic characteristics of sealing performance and the mesoscopic flow field, the macroscopic performance parameters (opening force and leakage rate) and the mesoscopic velocity components were subject to the same rotation speed change for comparative analysis. Considering the obvious disturbance phenomenon under turbulence, the study mainly focused on the RNG turbulent regime. Meanwhile, given the linear relationship between circumferential velocity and rotation speed, the axial and radial velocity components were selected as the research objects in the mesoscopic flow field.

Fig. 14 shows the comparison results of the macroscopic performance parameters and corresponding velocity components based on the turbulent regime at different film thicknesses. It can be seen that the larger the film thickness, the more significant the fluctuation trend of the macro performance parameters when the rotation speed changes. The variation trend of the leakage rate and radial velocity component under different working conditions is basically the same and their inflection point (the abbreviation in the figure is IP1 and IP2) values are also real-time and one-to-one corresponding, indicating that the change in leakage rate is an immediate and macroscopic reflection of the radial velocity component and

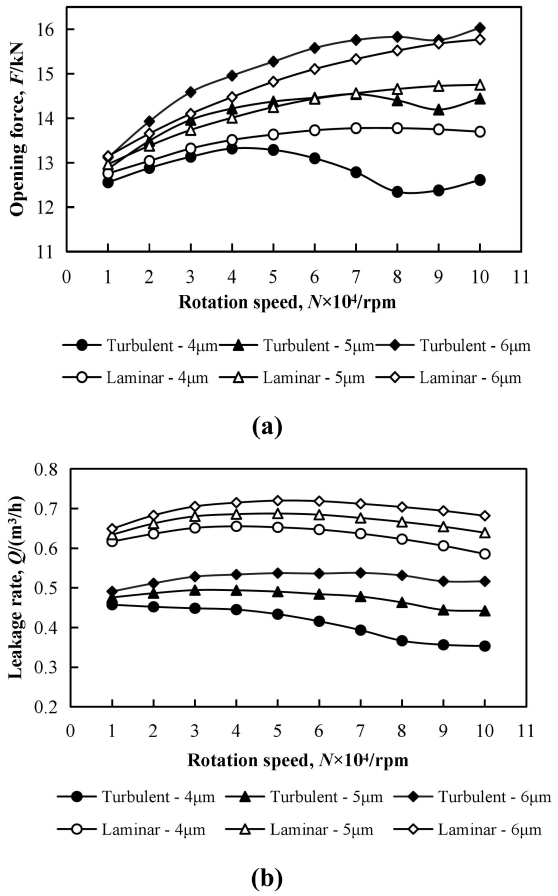

FIGURE 13. Performance comparison of two flow regimes at different groove depths (P_{in} = 2MPa, $h = 5\mu$m); (a) effect of the groove depth change on the opening force; (b) effect of the groove depth change on the leakage rate.

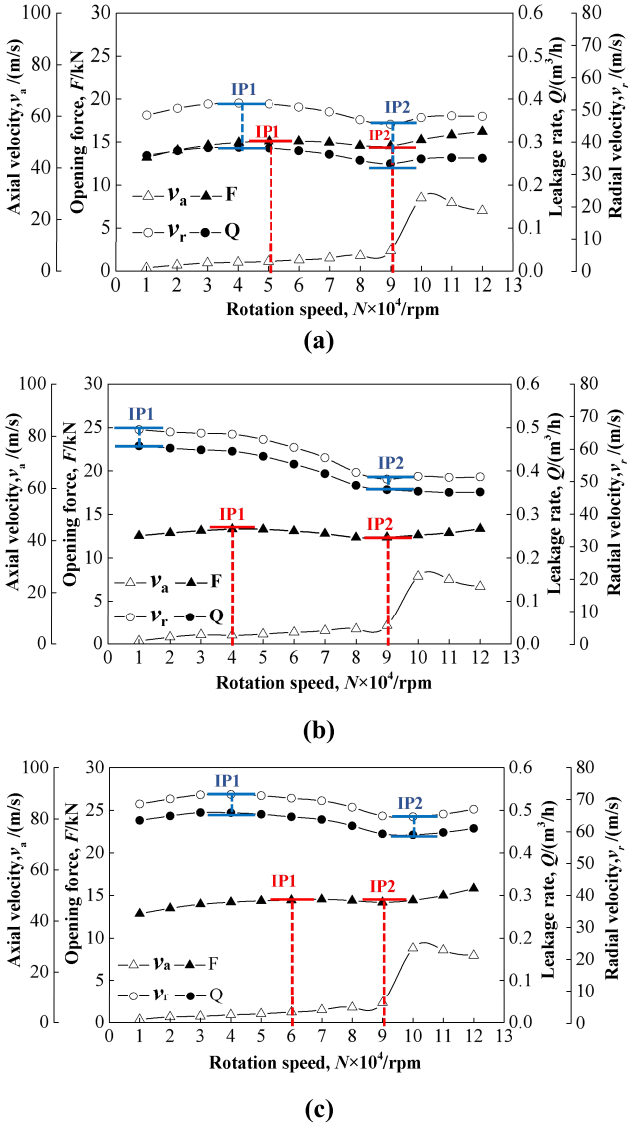

FIGURE 14. Comparative analysis of the macroscopic performance and mesoscopic velocity components at different rotation speeds (P_{in} = 2MPa); (a) $h = 4\mu$m, $h_g = 4\mu$m; (b) $h = 5\mu$m, $h_g = 4\mu$m; (c) $h = 5\mu$m, $h_g = 5\mu$m.

the latter is also a direct internal factor of the change in the former. Compared to the instantaneous feedback relationship between leakage rate and radial velocity, the evolutionary relationship between the opening force and axial velocity component is not completely consistent but both tend to increase with the increase in rotation speed.

Notably, the axial velocity component will suddenly increase during the process of a continuous increase in the rotation speed and the mutation point corresponds to the rotation speed of the macroscopic second inflection point ($N = 9 \times 10^4$ rpm). This result shows that the axial velocity component can better reflect the fluctuation of the entire flow field, namely when the axial velocity component increases to a certain value or mutate, it suggests that the entire flow field has undergone significant fluctuations, such as transitions, vortexes, and other phenomena.

VI. ROTATING FLOW REGIME DECISION MODEL

A. MATHEMATIC MODEL

The aforementioned research shows that the fluid flow in the high-speed rotating flow field is very complex and the influence of the axial velocity component must be considered in the analysis of the flow regime. Based on the two-dimensional parametric Oval model of the flow factor, and according to the internal logical relation and evolutionary law of disturbance generation and axial velocity components, an ellipsoid decision model of three-dimensional velocity components considering circumferential, radial, and axial directions is proposed as follows:

$$\lambda = \sqrt{\left(\frac{Re_c}{1600}\right)^2 + \left(\frac{Re_p}{2300}\right)^2 + \left(\frac{Re_a}{X}\right)^2} \tag{12}$$

$$\begin{cases} Re_c = \dfrac{\rho v_c L_{Hc}}{\mu} & (13a) \\ Re_p = \dfrac{\rho v_r L_{Hp}}{\mu} & (13b) \\ Re_a = \dfrac{\rho v_a L_{Ha}}{\mu} & (13c) \end{cases}$$

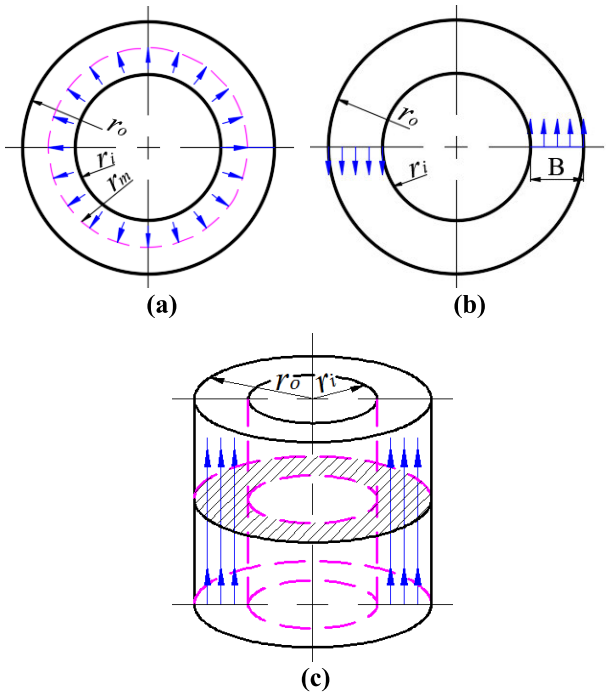

FIGURE 15. Hydraulic diameter calculation model: (a) circumferential model, (b) radial model, (c) and axial model.

$$\begin{cases} L_{Hp} = 4\dfrac{A_p}{S_p} = 4\dfrac{\pi 2 r_m h}{2\pi 2 r_m} = 2h & (14a) \\ L_{Hc} = 4\dfrac{A_c}{S_c} = 4\dfrac{Bh}{2B} = 2h & (14b) \\ L_{Ha} = 4\dfrac{A_a}{S_a} = 4\dfrac{\pi\left(r_o^2 - r_i^2\right)}{2\pi\left(r_o + r_i\right)} = 2B & (14c) \end{cases}$$

As shown in (12), compared with the 2D flow factor decision model, the 3D Ellipsoid model not only includes the Re_c and Re_p of the Reynolds number when Couette shear flow and Poiseuille radial pressure flow are considered separately, but also considers the influence of Re_a of the Reynolds number when axial flow is considered. Series (13) are shown as the calculation models corresponding to three kinds of Reynolds Numbers. The definition of characteristic size L is very important for the model. According to the basic principle of hydromechanics, the hydraulic diameter L_H is selected as the characteristic size in each Reynolds number model, and the specific expression is 4 times of the ratio of the cross section area A to the cross section circumference S, as shown in series (14).

Fig. 15 (a) and (b) respectively show the hydraulic diameter calculation models of circumferential and radial velocity components, which are one-to-one corresponding to 15(a) and (b). Where, B is the width of the sealing ring, and r_m is the average radius of the calculated region.

In (12), we can regard Re_a as the Perturbation Reynolds number, whose value is undetermined, and X is the critical Reynolds number corresponding to the undetermined Re_a. For a DGS, the axial velocity component here is along the direction of the gas film thickness, which can be analogous to a pipeline model. According to the theory of fluid mechanics, X can be taken as the critical turbulent Reynolds number 4000, as shown in Fig. 15 (c).

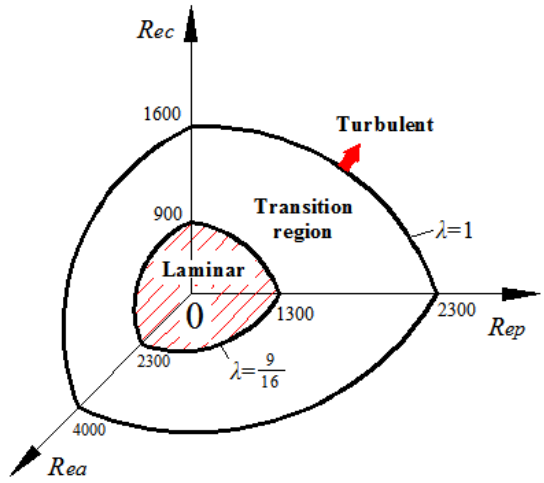

FIGURE 16. Rotating flow field three-dimensional decision model (Ellipsoid model).

TABLE 4. Orthogonal test factor table.

Factors	values			
h/μm	3	4	5	6
h_g/μm	2	3	4	5
P_{in}/MPa	1	2	3	4

TABLE 5. Validation group (post-transition).

Groups	h /μm	h_g /μm	P /MPa	λ	The speed value corresponding to the inflection point N/rpm
A	3	2	1	4.01	6×10^4
B	3	3	2	6.19	8×10^4
C	3	4	3	4.29	7×10^4
D	3	5	4	3.61	6×10^4
E	4	2	2	3.64	4×10^4
F	4	3	1	11.49	8×10^4
G	4	4	4	3.74	5×10^4
H	4	5	3	3.66	5×10^4
I	5	2	3	1.17	2×10^4
J	5	3	4	5.00	4×10^4
K	5	4	1	7.10	6×10^4
L	5	5	2	5.14	5×10^4
M	6	2	4	1.33	2×10^4
N	6	3	3	3.32	3×10^4
O	6	4	2	5.97	4×10^4
P	6	5	1	7.81	5×10^4

TABLE 6. Validation group (pre-transition).

N/rpm	Groups															
	A	B	C	D	E	F	G	H	I	J	K	L	M	N	O	P
1000	0.13	0.35	0.50	0.85	0.30	0.11	0.73	0.53	0.63	0.89	0.15	0.40	0.93	0.69	0.43	0.20
2000	0.13	0.36	0.51	0.86	0.30	0.12	0.73	0.53	0.63	0.89	0.15	0.40	0.93	0.69	0.43	0.16
3000	0.13	0.36	0.52	0.87	0.30	0.16	0.74	0.54	0.63	0.89	0.17	0.41	0.93	0.69	0.43	0.20
4000	0.19	0.37	0.52	0.87	0.30	0.24	0.75	0.55	0.63	0.89	0.26	0.41	0.93	0.69	0.43	0.28
5000	0.26	0.37	0.54	0.89	0.30	0.32	0.75	0.55	0.63	0.89	0.34	0.41	0.93	0.69	0.43	0.34
6000	0.33	0.38	0.54	0.90	0.30	0.39	0.75	0.55	0.63	0.89	0.40	0.42	0.92	0.69	0.43	0.40
7000	0.40	0.38	0.56	0.91	0.31	0.46	0.76	0.56	0.63	0.89	0.48	0.42	0.92	0.69	0.43	0.49
8000	0.46	0.39	0.56	0.93	0.36	0.54	0.76	0.57	0.63	0.89	0.56	0.44	0.92	0.69	0.43	0.63
9000	0.54	0.42	0.57	0.94	0.42	0.60	0.76	0.58	0.63	0.89	0.64	0.52	0.92	0.69	0.51	0.73

B. MODEL DESCRIPTION

According to (12), the corresponding decision model is a spatial isometric ellipsoid, as shown in Fig. 16, where $\lambda < 9/16$ denotes a laminar regime, $\lambda > 1$ denotes a turbulent regime, and $9/16 \leq \lambda \leq 1$ denotes a laminar to turbulent transitional region in which the disturbance factor in the flow field begins to appear.

C. MODEL VERIFICATION

In conclusion, the decision model is an ellipsoid space area. To test and verify the correctness of the model, the theoretical basis is as follows: On the one hand, there is no immediate correspondence between the generation of turbulence and macroscopic parameters such as opening force and leakage rate in the rotating flow field. On the other hand, if there is an inflection point for the opening force or leakage rate, then the condition is considered to have completed transition, i.e. the corresponding Ellipsoid model is $\lambda > 1$.

Based on this, the verification is divided into two parts: a pre-transition ($\lambda < 1$) verification and post-transition ($\lambda > 1$) verification. To render the verification results more reliable, a multi-factor problem verification scheme was established using an orthogonal test method, making the verification scheme more random. The detailed parameters are shown in Table 4.

According to Table 4, a total of 16 parameter groups can be obtained, as shown in Table 5. To ensure that the verification of the decision model covers the whole transition process, the rotation speed starts from 1000 rpm at the lowest and reaches to 1.0×10^5 rpm at the highest.

The expected results are summarized as follows:

At a low rotation speed (much lower than the inflection point value, i.e. before the transition), the corresponding calculation value should be located on the $\lambda < 1$ side.

The appearance of an inflection point indicates that a transition has occurred. At this point, the calculation value should be on the $\lambda > 1$ side (it is typically much greater than 1).

If the verification results are consistent with the aforementioned conclusions, the accuracy of the Ellipsoid model can basically be verified.

All the operational conditions shown in Table 5 have macroscopic inflection points, indicating that a transition has occurred, and the decision values are all greater than 1, which is consistent with the expected results.

Similarly, at a relatively low speed ($N \leq 9 \times 10^3$ rpm), a validation was conducted based on the same parameter. Theoretically speaking, at this time, there was no fluctuation in the macroscopic performance and mesoscopic flow field, that is, a transition did not occur; thus, the decision value should be less than 1. As shown in Table 6, the decision values calculated according to the Ellipsoid model are all less than 1 and the verification results are completely in line with the theoretical expectations. Based on this, it can be basically verified that the Ellipsoid model has good accuracy in determining the rotating flow field flow regime.

VII. CONCLUSION

To accurately determine the flow regime of a DGS microscale rotating flow field, this study introduced a new method (Ellipsoid model) based on a three-dimensional velocity component. The new model is based on the Pipe and Oval models but is more accurate than both.

The conclusions are as follows:

- The high operational condition of the DGS and the existence of a groove, dam, and weir result in an internal rotating flow field that is extremely complex. The traditional critical Reynolds number or flow factor cannot accurately determine the flow regime of a DGS flow field.
- The choice of a laminar or turbulent regime has great influence on the specific value of the sealing performance, but little influence on the variation trend and regularity of the related parameters.
- There are circumferential, radial, and axial velocity components in the rotating flow field at the same time.

The influence of the axial velocity component should be considered when the rotation speed is high. A continuous increase in the rotation speed will lead to a sharp increase in the axial velocity component in the flow field, which is the main factor leading to large fluctuations or inflection points in the macroscopic sealing performance (opening force and leakage rate).

- The Ellipsoid model can be used to determine the DGS flow regime and similar high-speed rotating flow fields and it agrees well with the actual situation.

REFERENCES

[1] R. P. Gabriel, "Fundamentals of spiral groove noncontacting face seals," *Lubrication Eng.*, vol. 50, no. 3, pp. 215–224, 1994.
[2] B. Ruan, "Finite element analysis of the spiral groove gas face seal at the slow speed and the low pressure conditions—Slip flow consideration," *Tribology Trans.*, vol. 43, no. 3, pp. 411–418, Jan. 2000.
[3] M. T. C. Faria, "An efficient finite element procedure for analysis of high-speed spiral groove gas face seals," *J. Tribology*, vol. 123, no. 1, pp. 205–210, Jan. 2001.
[4] S. Blasiak and A. V. Zahorulko, "A parametric and dynamic analysis of non-contacting gas face seals with modified surfaces," *Tribology Int.*, vol. 94, pp. 126–137, Feb. 2016.
[5] Y. Chen, X. Peng, J. Jiang, X. Meng, and J. Li, "Experimental and theoretical studies of the dynamic behavior of a spiral-groove dry gas seal at high-speeds," *Tribology Int.*, vol. 125, pp. 17–26, Sep. 2018.
[6] N. Zirkelback, "Parametric study of spiral groove gas face seals," *Tribology Trans.*, vol. 43, no. 2, pp. 337–343, Jan. 2000.
[7] G. Ma, W. Zhao, and X. M. Shen, "Analysis of parameters and performance for spiral grooved cylindrical gas film seal," *Procedia Eng.*, vol. 23, pp. 115–119, Jun. 2011.
[8] J. A. Yasuna and W. F. Hughes, "Squeeze film dynamics of two-phase seals: Part II—Turbulent flow," *J. Tribology*, vol. 116, no. 3, pp. 479–487, Jul. 1994.
[9] G. Ma, W. Zhao, and X. M. Shen, "Three dimensional numerical simulation on the micro-gap flow field of spiral groove gas film seal," *Lubrication Eng.*, vol. 37, no. 3, pp. 7–11, Mar. 2012.
[10] I. Shahin, M. Gadala, M. Alqaradawi, and O. Badr, "Three dimensional computational study for spiral dry gas seal with constant groove depth and different tapered Grooves," *Procedia Eng.*, vol. 68, pp. 205–212, Dec. 2013.
[11] D. L. Ransom and L. San Andrés, "Identification of force coefficients from a gas annular Seal–Effect of transition flow regime to turbulence," *Tribology Trans.*, vol. 42, no. 3, pp. 487–494, Jan. 1999.
[12] J. J. Sun, C. B. Ma, Q. P. Yu, J. H. Lu, M. Zhou, and P. Y. Zhou, "Numerical analysis on a new pump-out hydrodynamic mechanical seal," *Tribology Int.*, vol. 106, pp. 62–70, Jun. 2017.
[13] J. Jiang, X. Peng, J. Li, and Y. Chen, "A comparative study on the performance of typical types of bionic groove dry gas seal based on bird wing," *J. Bionic Eng.*, vol. 13, no. 2, pp. 324–334, Jun. 2016.
[14] B. Wang, H. Zhang, and H. Cao, "Flow dynamics of a spiral-groove dry-gas seal," *Chin. J. Mech. Eng.*, vol. 26, no. 1, pp. 78–84, Jan. 2013.
[15] X. X. Ding, P. G. Zhang, Y. F. Huang, and J. Zheng, "Numerical simulation of computational fluid dynamics (CFD) of the microscale flow field in the spiral groove dry gas seals," *CIESC J.*, vol. 36, no. 5, pp. 287–290, Oct. 2008.
[16] Y. Wang, H. Yang, J. Wang, Y. Liu, H. Wang, and X. Feng, "Theoretical analyses and field applications of gas-film lubricated mechanical face seals with herringbone spiral grooves," *Tribology Trans.*, vol. 52, no. 6, pp. 800–806, Oct. 2009.
[17] H. Su, R. Rahmani, and H. Rahnejat, "Thermohydrodynamics of bidirectional groove dry gas seals with slip flow," *Int. J. Thermal Sci.*, vol. 110, pp. 270–284, Dec. 2016.
[18] N. Brunetière, B. Tournerie, and J. Frêâe, "Influence of fluid flow regime on performances of non-contacting liquid face seals," *J. Tribology*, vol. 124, no. 3, pp. 515–523, Jul. 2002.
[19] Z. M. Fairuz and I. Jahn, "The influence of real gas effects on the performance of supercritical CO_2 dry gas seals," *Tribology Int.*, vol. 102, pp. 333–347, Oct. 2016.
[20] H. L. Chen, Q. Wang, W. Y. Li, and J. J. Zhang, "Numerical simulation of 3-D flow in upstream pumping mechanical seals with spiral grooves based on Fluent," *Lubrication Eng.*, vol. 37, no. 2, pp. 16–19, Feb. 2012.
[21] X. W. Jiang and B. Q. Gu, "Characteristic of gas film between spiral groove dry gas seal faces," *Chin. J. Chem. Eng.*, vol. 56, no. 8, pp. 1419–1425, Aug. 2005.
[22] H. J. Xu, P. Y. Song, W. Y. Mao, Q. G. Deng, and X. J. Sun, "Analysis on inertia effect of carbon dioxide dry gas seal at high speed and pressure under laminar condition," *CIESC J.*, vol. 69, no. 10, pp. 4311–4323, Jul. 2018.
[23] X. X. Ding, Y. J. Fu, J. Zhang, W. Z. Zhang, and S. R. Yu, "Fluid state analysis on flow field of gas seal with spiral groove based on CFD," *J. Drainage. Irrigation. Mach. Eng./Paiguan Jixie Gongcheng Xuebao*, vol. 28, no. 4, pp. 330–334, Jul. 2010.
[24] Y. Wang, Q. Hu, Y. X. Xiao, G. Q. Huang, Y. H. Zhu, and Y. L. Ge, "Turbulence effect and suppression mechanism of dry gas seal at ultra-high speeds," *Acta Aeronaut. Astronaut. Sin.*, vol. 40, no. 10, pp. 116–125 Jul. 2019.
[25] B. Wang, "Numerical analysis of a spiral-groove dry-gas seal considering micro-scale effects," *Chin. J. Mech. Eng.*, vol. 24, no. 1, p. 146, 2011.
[26] Y. Wang, J. J. Sun, Q. Hu, D. Wang, and X. Q. Zheng, "Orientation effect of orderly roughness microstructure on spiral groove dry gas seal," *Tribology Int.*, vol. 126, no. 6, pp. 97–105, Oct. 2018.
[27] J. Xie and S. X. Bai, "The effect of high speed airflow lubrication on hydrodynamic properties of inclined-dimples face seals," *Tribology*, vol. 37, no. 6, pp. 806–813, Jul. 2017.
[28] V. Yakhot and S. A. Orszag, "Renormalization group analysis of turbulence.I. Basic theory," *J. Sci. Comput.*, vol. 1, no. 1, pp. 3–51, May 1986.
[29] Y. Wang, J. J. Sun, K. Tao, C. B. Ma, and Q. A. Tu, "Numerical analysis of T-groove dry gas seal and groove optimization," *Tribology*, vol. 34, no. 4, pp. 420–427, Jul. 2014.
[30] X. N. Yin and X. D. Peng, "Selection of a shape function in finite element analysis for a spiral groove dry gas seal," *Lubrication Eng.-Huangpu*, vol. 175, no. 3, p. 13, Mar. 2006.

YAN WANG is currently pursuing the Ph.D. degree. He is also an Associate Professor with Jiangsu Ocean University. He has presided over two projects of the National Natural Science Foundation of China and one project of the Natural Science Foundation of Jiangsu Province. The seal in the non-contacting mechanical (dry gas seal) groove is further studied by Yan Wang and obtained a variety of new types of groove with excellent performance, theory, and experiment as, for the sealing groove, processing technology was also explored, and some achievement was obtained. He holds two patents. His research fields mainly focus on fluid mechanical seal and dry gas sealing technology.

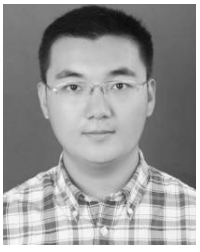

YUNLU GE graduated from Jiangsu Ocean University, in 2018, where he is currently pursuing the degree. The tutor is Dr. Yan Wang. He has participated in the Natural Science Foundation of Jiangsu. His research direction is in fluid mechanics and sealing technology.

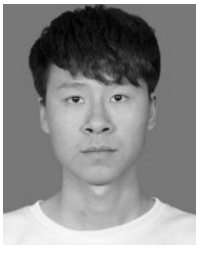

GUOQING HUANG graduated from Jiangsu Ocean University, in 2018, where he is currently pursuing the degree. The tutor is Dr. Qiong Hu. He has participated in the Natural Science Foundation of Jiangsu. His research direction is in fluid mechanics and sealing technology.

QIONG HU received the Ph.D. degree in mechanical engineering from Nanjing Forestry University, Jiangsu, China, in 2016. She worked as an Engineer with NGC, Jiangsu, until March 2018. She has a half-year experience of studying with the Department of Mechanical Engineering, Louisiana State University. She is currently a Lecturer and teaches several professional courses of mechanical engineering with Jiangsu Ocean University, Jiangsu. She has published 14 research articles in the journals. Her research interests include fluid sealing technology, tribology, numerical simulations, and heat transfer.

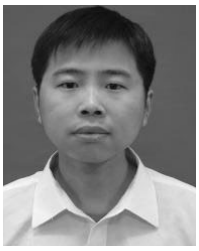

PENG HU was born in Lianyungang, Jiangsu, China, in 1986. He received the Ph.D. degree in mechanical design and theory from the School of Mechanical Engineering and Automation, Northeastern University, Shenyang, Liaoning, China, in 2020. He is currently a Lecturer with Jiangsu Ocean University, Jiangsu, China.